Composites Science and Technology 243 (2023) 110236

Contents lists available at ScienceDirect

Composites Science and Technology

journal homepage: www.elsevier.com/locate/compscitech

The micromechanics of graphene oxide and molybdenum disulfide in thermoplastic nanocomposites and the impact to the polymer-filler interphase

Josué Marciano de Oliveira Cremonezzi [a,b,c], Gabriel Matheus Pinto [a,b], Rosica Mincheva [c], Ricardo Jorge Espanhol Andrade [a,b], Jean-Marie Raquez [c], Guilhermino José Macedo Fechine [a,b,*]

[a] MackGraphe – Mackenzie Institute for Graphene and Nanotechnology, Rua da Consolação, 896 – Consolação, São Paulo, SP, 01302-907, Brazil
[b] School of Engineering, Mackenzie Presbyterian University, Rua da Consolação, 896 – Consolação, São Paulo, SP, 01302-907, Brazil
[c] Laboratory of Polymeric and Composite Materials, Center of Innovation and Research in Materials and Polymers (CIRMAP), University of Mons, Place du Parc 20, 7000, Mons, Belgium

ARTICLE INFO

Handling Editor: Marino Quaresimin

Keywords:
Graphene and other 2D-materials (A)
Nanocomposites (A)
Polymer-matrix composites (PMCs) (A)
Mechanical properties (B)
Interphase (B)

ABSTRACT

The addition of two-dimensional nanomaterials to a polymer matrix is a widely known manner to mechanically reinforce the material. The stress-transfer in the polymeric matrices, however, depends on an array of filler and matrix properties as well as on their interface. In this work, we discuss the effects of the distinct levels of interaction of graphene oxide, reduced graphene oxide and molybdenum disulfide with poly(vinyl butyral) in the reinforcement of the polymer. For that, we employed the micromechanical analysis model originally developed by Young et al., which describes the reinforcement behavior of graphene nanoplatelets in a wide range of polymer matrices. Then, using an innovative approach derived from such analysis, we propose novel methods to mathematically evaluate the effects of the filler content upon the polymer/filler interface, and for the determination of the mechanical percolation threshold.

1. Introduction

Poly(vinyl butyral) (PVB) is a terpolymer formed by randomly arranged vinyl butyral (VB), vinyl alcohol (VA), and vinyl acetate (VAc) monomers, with properties varying according to the proportion of these monomers in its structure. While VB monomers are hydrophobic, granting elasticity, toughness, and compatibility with various plasticizers to the polymer, VA provides adhesion to inorganic materials [1]. Moreover, the hydroxyl side group of the VA units is a suitable site for hydrogen bonding [2,3], acting as a physical crosslinking and leading to chain entanglement [4–6]. Windshield grade PVB has a considerable amount of plasticizer in its composition, 25 to 30 wt%, that lowers the polymer glass transition temperature to 16–18 °C [7], and make it to present an elastomer-like tensile behavior [8–10]. The main PVB application is as the intermediate layer of laminated glass, with automotive and civil construction industries accounting for 52 and 43% of its worldwide consumption. Nonetheless, the clean energy sector is considered an emerging field for PVB due to its adoption in the encapsulation of photovoltaic cells and glasses [11].

Several nanofillers have already been reported to enhance diverse PVB properties [12–16]. However, graphene oxide (GO) has been identified as the most efficient to reinforce PVB [17]. The better efficiency of GO was attributed to the interactions between the filler's oxygenated groups and polymer matrices. Hajian et al. [18] employed GO to enhance not just mechanical properties of PVB, but its thermal stability as well. The addition of small amounts of GO, from 0.1 to 0.6 wt %, was enough to improve the thermal stability of the polymer. In terms of mechanical reinforcement, with only 0.1 wt%, Young's modulus and tensile strength increased by 48.7% and 27.3%, respectively. The authors attributed these improvements to the high aspect ratio of GO, uniform dispersion in the matrix, and strong interactions between the nanofiller and the polymer. Differently from graphene, which is well known to be inert to polymers [19], the oxygenated groups that decorate the GO surface tend to generate stronger interactions with the matrix,

* Corresponding author. MackGraphe – Mackenzie Institute for Graphene and Nanotechnology, Rua da Consolação, 896 – Consolação, São Paulo, SP, 01302-907, Brazil.
E-mail address: guilherminojmf@mackenzie.br (G.J.M. Fechine).

https://doi.org/10.1016/j.compscitech.2023.110236
Received 2 May 2023; Received in revised form 1 August 2023; Accepted 23 August 2023
Available online 24 August 2023

improve filler dispersion and, consequently, facilitate stress transfer [20,21].

Another interesting class of nanomaterials to be employed as reinforcement for PVB is transition metal dichalcogenides (TMD), among which molybdenum disulfide (MoS_2) is the most studied [22]. The great interest comes from the fact that the mechanical properties of MoS_2 are comparable to those of GO. Moreover, the polarity of the sulfur surface of MoS_2 may lead to interactions with polymers [23–25]. Wang et al. [23] showed that polyurethane chains were adsorbed on the surface of MoS_2 nanoplatelets via hydrogen bonding, generating nanoconfined regions, which increased the effective volume fraction of the reinforcement. As a result, the stress transfer from the polyurethane matrix to the nanofiller was highly efficient.

Within that scope, the development of polymer composites enhanced by 2D nanomaterials is reaching a high degree of technological maturity. Since the emergence of the pioneering graphene-based polymer nanocomposite [26], many advances were achieved, and the main challenges are now being addressed on how to adopt these nanomaterials at the industrial level in different applications [27–30]. However, the successful mechanical performance of polymer artefacts depends on the reinforcement of the filler, the matrix, and the interface. Thus, variables such as the filler's size, dispersion, and surface properties directly interfere in the reinforcement efficiency, making the mathematical assessment and manipulation of the behavior and features of a given nanocomposite still a challenge to be addressed [28,31].

In this sense, Young et al. [32] has proposed a micromechanical analysis-based model, derived from the shear-lag theory, capable to predict the stiffening effect of graphene nanoplatelets (GNP) in polymeric nanocomposites. The model showed an excellent agreement with the experimental results achieved in the case of composites made of polymeric matrices of different stiffness. The efficiency of filler reinforcement [33], percolation threshold [34], filler confinement [35], and agglomeration [36] could be discussed by Young's group under the light of the proposed model, but there is still space to increase the applicability of the model, as shown in this work.

Herein, we evaluated the effect of the polar interactions between two distinct nanofillers, i.e., graphene oxide and MoS_2 with a PVB matrix in its mechanical reinforcement. The interactions between PVB and GO or MoS_2 were assessed using Fourier transform infrared (FTIR) and thermogravimetric analysis (TGA). Reduced graphene oxide (rGO) was also employed to complement the observations. It was verified that the higher the polymer/filler interactions, the better the filler dispersion and mechanical reinforcement. The PVB/GO and PVB/MoS_2 microstructures' analyses through scanning transmission electron microscopy (STEM) and X-ray diffraction (XRD) was employed to support such a hypothesis.

Finally, the micromechanical analysis was employed in an innovative way to assess the extent of the polymer/filler interphase upon the volumetric fraction of these nanofillers. The observed interphase behavior with the volumetric fraction of the filler enabled us to propose a novel approach for the determination of the mechanical percolation threshold within the matrix. The results agreed with the observed in both mechanical and dynamic mechanical analyses of the corresponding nanocomposites.

2. Materials and methods

2.1. Materials

Graphene oxide was exfoliated in absolute ethanol (LabSynth) at a concentration of 1 mg mL^{-1} in an ultrasound bath for 180 min from a graphite oxide (GrO) produced in a process development reactor [37]. Aiming to compare PVB/GO and PVB/rGO interactions, rGO was synthesis procedure is detailed and briefly discussed in Appendix A (Fig. S1). MoS_2 was obtained from the liquid exfoliation of molybdenum (IV) disulfate powder (Sigma-Aldrich, particle size of ~6 μm) under the same conditions as GO.

PVB films from the glass lamination waste were provided by Inbra-Filtro Ind. e Com. de Filtros Ltda after being granulated in a knife mill. Nanocomposites were obtained by solution casting of the granulated polymer with GO or MoS_2 in absolute ethanol for 24 h under stirring. Films with a thickness of ~0.7 mm were obtained by casting the polymer nanocomposite solutions in glass molds, followed by solvent evaporation for 21 days under ambient conditions. The mass fraction (w_f) and volume fraction (φ_f) of the obtained nanocomposites are summarized in Table S1.

2.2. Characterization methods

GO and MoS_2 characterization was performed according to a protocol discussed elsewhere [38]. Nevertheless, the relevant aspects of the employed nanofillers are shown in Appendix A (Figs. S2–3).

Films were analyzed by XRD in a MiniFlex II (Rigaku) diffractometer, using CuK α radiation, 0.02 step, and a scan rate of 1 min^{-1}. FTIR spectroscopy was performed on a Tensor 27 (Bruker) spectrometer with a resolution of 2 cm^{-1}. TGA was performed in a thermal analyzer model TGA Q500 (TA Instruments®) with a 20 °C min^{-1} heating ramp in a nitrogen atmosphere. Tiny portions of each film were cut in a microtome and analyzed in a Hitachi SU8020 ultrahigh resolution scanning electron microscope for STEM with an acceleration voltage of 30 kV.

For dynamical mechanical analysis (DMA), 0.7 mm thick ribbons were cut from the films and evaluated on a DMA Q800 (TA Instruments®) in the tensile mode under 1% strain at a frequency of 1 Hz and a temperature ramp of 2.5 C min^{-1}. The length of the specimens was chosen considering a geometry factor of 2. At least seven dumbbell-shaped specimens of each composition were extracted from the films for the tensile test, performed on a universal QTEST (MTS® Systems) testing machine according to ASTM D 638 under 50 mm min^{-1} deformation. The fracture surface of the specimens was covered with gold via sputtering and analyzed by scanning electron microscopy (SEM) in a JSM-6510 (Jeol) scanning electron microscope with a secondary electron detector and an acceleration voltage of 25 kV.

2.3. Data analysis

Whenever possible, the measures are reported in a confidence interval as $\overline{x} \pm u$, where $\overline{x}$ is the mean measured value and u is the uncertainty calculated as the Student's t-distribution with α equal to 0.05 (95% of confidence) times the standard deviation divided by the square root of the number of values in the sample. Tensile test results were analyzed using one-way analysis of variance (ANOVA) test and the Tukey's honestly significant difference (THSD) post hoc test with a simultaneous confidence level of 95% ($P < 0.05$) using the Minitab 17 (Minitab) software.

3. Results

Hydrogen bonding was the type of interaction expected to occur between PVB and the nanofillers employed. As already mentioned, the hydroxyl side group of the PVB structure is a suitable site for this kind of interaction [2,3], which has been observed between both GO and MoS_2 for polymers such as poly(vinyl alcohol) [3,24], polyurethanes [23,39], and poly(ether sulfone) [25]. The polymer/nanofiller interaction was therefore assessed by FTIR and TGA, as deeply discussed in Appendix A (Figs. S4–7). Results indicated that GO presented a strong interaction with PVB via hydrogen bond, confirming the expectations [17,18,20,21]. With rGO, which had less oxygenated groups available, the interaction level with the polymer was lower than with GO. MoS_2, in turn, had even poorer interaction with the polymer, despite the evidence from other works [23–25].

3.1. Nanocomposites' microstructure

The distinct levels of polymer/filler interactions verified in the case of PVB/GO and PVB/MoS_2 led to different microstructures. As can be seen in the STEM images shown in Fig. 1, even with the increasing filler content, GO was well dispersed in the PVB/GO nanocomposites with 0.05, 0.25, and 1.50 wt%. On the other hand, as the filler content increased in PVB/MoS_2 composites from 0.10 to 0.50 and 1.50 wt%, aggregates were formed. Consequently, MoS_2 presented a poor dispersion in PVB. The STEM images were also useful to verify that both fillers presented a random orientation, which is an important input for the following theoretical discussion.

The difference in the dispersion of GO and MoS_2 in PVB was also evidenced by XRD. The (002) diffraction peak that GO exhibits at 10.2° [40] did not appear in the diffractograms of the PVB/GO nanocomposites (Fig. S8a). The diffractograms of PVB/MoS_2 nanocomposites (Fig. S8b), in turn, had several MoS_2 peaks. The major evidence of the restacking of MoS_2 flakes was the emergence of the (103) and (105) diffraction peaks, typical of the bulk MoS_2 and not of the exfoliated [38].

3.2. Dynamic mechanical analysis

The structural differences of PVB/GO and PVB/MoS_2 led to different dynamic mechanical properties. Fig. 2a shows that GO enhanced the storage modulus (E') of the polymer in the glassy state (−20 °C) regardless of filler content. From the loss factor ($\tan\delta$) curve, it was possible to see that the damping property of the polymer was enhanced for most compositions, becoming lower than the neat PVB only above 1.00 wt%. Both results imply that GO nanosheets increased the internal friction of PVB [41], which again might be related to the H-bonding between filler and polymer. Fig. 2b reports the Cole-Cole plot, i.e., the loss factor as a function of the storage modulus for the PVB/GO nanocomposites. The presented diagrams were imperfect semicircles, indicating heterogeneity in the system, but the shape of the curves pointed towards a good polymer-filler interaction [42]. Moreover, the area under the curve increased with w_f up to 1.00% and decreased at higher loading, indicating that a better reinforcement effect was obtained with w_f of around 1.00%. The PVB/MoS_2 nanocomposites' dynamic properties were similar to those of PVB/GO. However, the composition that showed the biggest enhancement in E' in the glassy state (Fig. 2c) and the largest area under the Cole-Cole plot (Fig. 2d), was the one with w_f of 0.50%.

3.3. Tensile test and fractography

Fig. 3a and b shows the tensile curves of PVB/GO and PVB/MoS_2, respectively. The typical outcome of the reinforcement of polymers by two-dimensional nanomaterials is increases in stiffness and mechanical resistance, as they act as barriers for the crack propagation. However, these improvements are usually accompanied by a decrease in the ductility due to the interlocking of the polymeric chains [43,44]. As shown in Figs. S9a–b, GO led to the expected decrease in strain, confirming the chains interlocking effect. On the other hand, MoS_2 showed tendencies of a slight increase in strain and decrease in strength. This effect presented by MoS_2 as PVB nanofiller was similar to the elucidated by Ferreira et al. [45,46], which may be the result of the formation of agglomerates that cause a lubricant effect during deformation due to the incommensurable contact between the particles. In turn, rGO did not affect the mechanical properties of PVB, probably, due to the poor polymer/filler interactions. Figs. S9a–c exhibits the properties achieved by the PVB/rGO systems.

Nevertheless, GO and MoS_2 led to a remarkable increment of Young's modulus, as shown in Fig. 3c. The stiffness of PVB/GO increased with w_f while the stiffest PVB/MoS_2 nanocomposite was that with only 0.05 wt %. It is noteworthy that the Young's modulus of PVB/GO with 1.50 wt% was not statistically different from the one with 1.00 wt%. Therefore, in terms of efficiency, 1.00 wt% seems to be the ideal GO concentration for PVB mechanical reinforcement, corroborating with the results from DMA. For PVB/MoS_2, it must be highlighted that, although the stiffness of the nanocomposite decreased with the increase of w_f, the moduli of the nanocomposites with w_f up to 0.50% were significantly higher than that of neat PVB.

SEM images of the tensile fracture surface of the nanocomposites are shown in Fig. S10. When the images of PVB and nanocomposites are compared, it is possible to see that both nanofillers led to an increase in the corrugated area of the surface. This indicates that the crack found a more tortuous path, requiring more energy to propagate, and, consequently, that new fracture-resistant mechanisms were present in the nanocomposites [47,48]. This is clearly seen by comparing the SEM images of the probable end-of-the-fracture regions of the PVB and nanocomposites with w_f of 1.00 wt%, as shown in Fig. 4. It is possible to see that, in neat PVB, the fracture propagated with high energy finding almost no barriers. This resulted in a smooth surface caused by a fracture with low energy dissipation. On the other hand, the very rough fracture surface of the nanocomposites indicates that the energy required for the crack to propagate was higher than in PVB, leading to plastic deformation at several points of the surface [43]. Moreover, once again, the distinct dispersion levels of GO and MoS_2 were apparent. As GO was

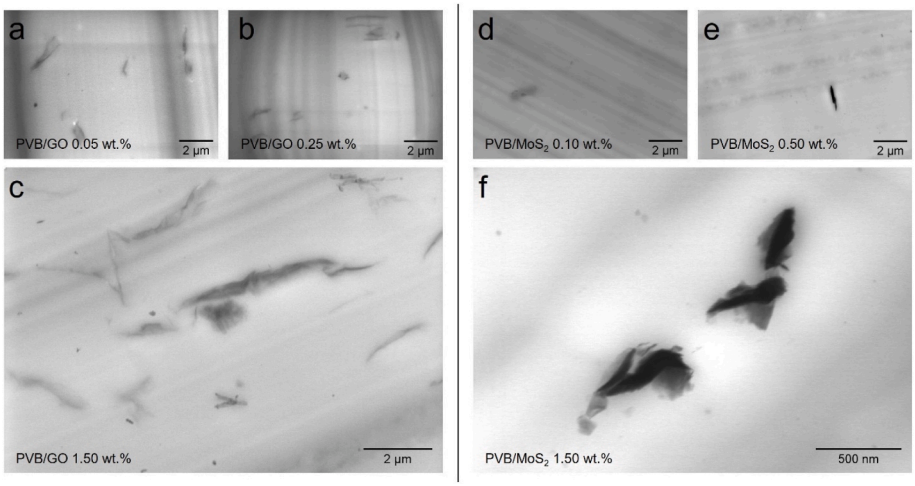

Fig. 1. STEM images of a-c) PVB/GO and d-f) PVB/MoS_2 nanocomposites in low, medium, and high filler proportion.

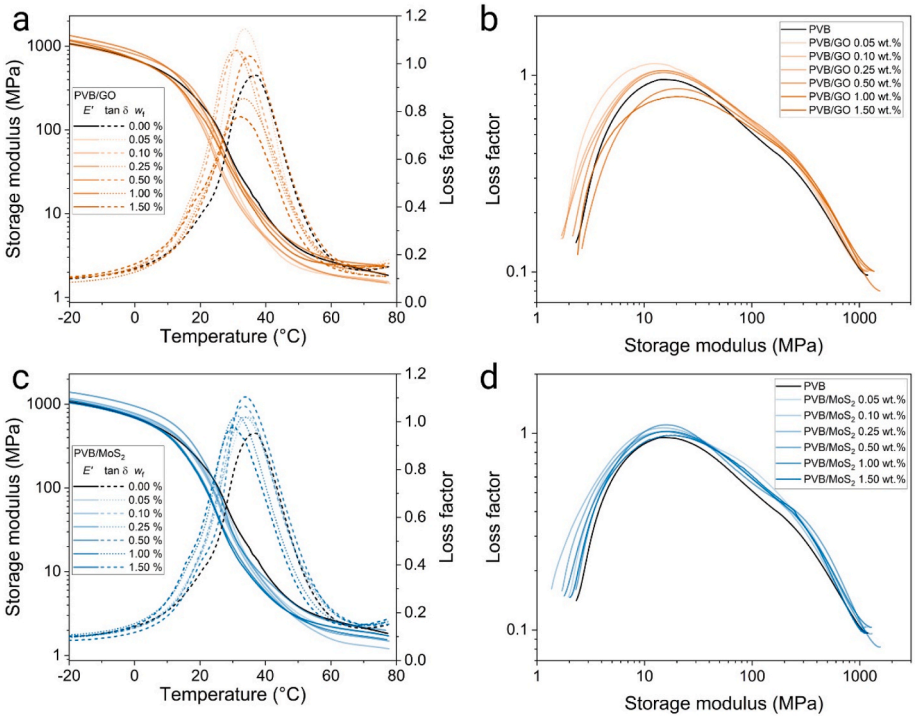

Fig. 2. a) Storage modulus and b) loss factor of PVB/GO; c) Storage modulus and d) loss factor of PVB/MoS_2.

better dispersed than MoS_2, more barriers for crack propagation were available, leaving a rougher aspect on the fracture surface.

4. Discussion

The micromechanics-based model proposed by Young et al. [32] departs from the classical rule of mixtures, shown in Equation (2), where E_c, E_f and E_m are the composite, filler, and matrix Young's moduli, and φ_f is the filler volumetric fraction.

$$E_c = E_f\varphi_f + E_m(1-\varphi_f) \tag{2}$$

Going further, those authors showed that when the filler is nanoplatelet-like, E_f depends on the orientation and size of the particle, according to Equation (3), where E_{eff} is the effective Young's modulus of the filler, η_o is the Krenchel orientation factor, and the η_l is the filler length factor.

$$E_f = E_{eff}\eta_o\eta_l \tag{3}$$

The η_o varies from 8/15 for randomly oriented to 1 for highly oriented particles while the η_l goes from 0 to 1, according to Equation (4), where s and t are the aspect ratio and the thickness of the nanoparticles; G_m, E_m and ν are the matrix shear and Young's moduli, and Poisson's ratio, respectively; and T is the thickness of the polymer/filler interphase.

$$\eta_l = \left[1 - \frac{\tanh(ns/2)}{ns/2}\right] \text{ where } n = \sqrt{\frac{2G_m}{E_{eff}}\frac{t}{T}} \text{ and } G_m = \frac{E_m}{2(1+\nu)} \tag{4}$$

By applying in Equation (3) the parameters listed in Table S2 along with an assumed t/T factor of the order of 10^{-2}, which will be discussed in the following, the theoretical E_f for GO and rGO would be 1.87 GPa, and for MoS_2 it would be equal to 0.20 GPa in the PVB matrix. However, as shown in Fig. S11a, there was a discrepancy between the predictions made through Equation (2) for the nanofillers E_f for a large interval of E_m (continuous lines) and the experimental results (points) obtained from the slope of the curves [32] shown in Fig. S12. Hence, the consideration of the filler's size and orientation effect was not enough for the model to be applicable to GO, rGO, and MoS_2.

4.1. Polymer/filler agglomeration coefficient

Such a discrepancy corroborated with the observed by Li et al. [36], who noticed that distinct levels of dispersion of the fillers led to different reinforcement effect. Therefore, according to them, the filler volumetric fraction factor should be instead an effective volume fraction (φ_{eff}) parameter to consider an agglomeration factor (η_a), turning Equation (2) into Equation (5). According to them, η_a varies from 0 to 1 meaning that η_a equals to 0 when the nanoparticles are agglomerated and no longer acting as nanoflakes but a bulk filler instead; and equals to 1 when they are well dispersed and in good interaction with the polymer matrix to enable efficient stress transfer.

$$E_c = \eta_o\eta_l E_{eff} \bullet \eta_a\varphi_f + E_m(1-\varphi_f) \tag{5}$$

From our observation, the interactions between the GO oxygenated groups and the polymer were of crucial importance to sustain a good dispersion of the filler and ensure mechanical reinforcement to PVB. On the other hand, MoS_2 stiffened the polymer, but the low interaction with the matrix, made the nanofiller dispersion to be precarious as the filler volumetric fraction increased, leading to a decay in the reinforcement effect efficiency. Thus, the values of η_a of each sample were assessed by isolating the term in Equation (5). In this calculation, E_f was obtained for each nanocomposite sample using Equation (3), employing the parameters listed in Table S2 and assuming that t/T is virtually equal to φ_f [32]. As can be seen in Fig. 5a and b, η_a much higher than 1 was observed for the lowest filler volumetric fractions, once we employed much lower filler contents than Li et al. [36]. Nonetheless, as the φ_f increased causing the GO and MoS_2 agglomeration at some extent, η_a values decayed tending to 0. In the highest φ_f, η_a of 0.4 and 0.3 were found for PVB/GO and PVB/MoS_2, respectively. PVB/rGO η_a values are not shown, but as expected, they were close to 0 despite of the φ_f, reflecting the poor interaction between the filler and the polymer.

4.2. Interphase thickness

Going further in the theory, it was shown that for soft matrices, a simplification of the model can be assumed. Then, E_f may be determined

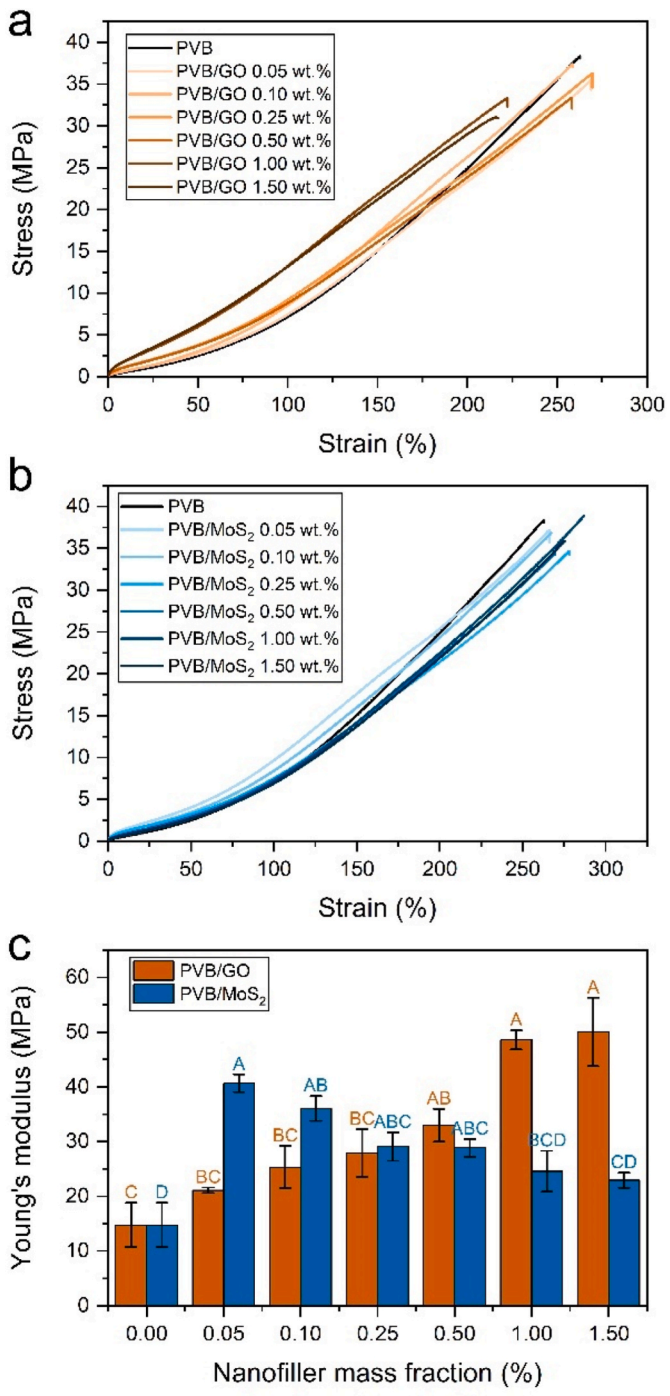

Fig. 3. Stress-strain curves of a) PVB/GO and b) PVB/MoS_2, and c) Young's moduli of the nanocomposites where letters represent the TSHD test grouping, meaning that values that do not share a letter are significantly different (only letters of the same color are comparable).

as presented in Equation (6) [32–34].

$$E_f \approx \eta_0 \frac{s^2}{12}\frac{t}{T}\frac{E_m}{(1+\nu)} \tag{6}$$

Moreover, by combining Equations (2) and (6) [32], one can predict the modulus of a nanocomposite through Equation (7).

$$E_c \approx E_m\left[1-\varphi_f+\frac{s^2}{12}\frac{t}{T}\frac{\eta_o}{(1+\nu)}\varphi_f\right] \tag{7}$$

The parameter t/T is a key element of the model. Analyzing the stress transfer from a matrix to a single flake with thickness t, one can see that the portion of the continuous matrix which can be affected by the flake is finite, with a thickness equal to T. The flake and the surrounding portion of the matrix, which is the interphase, form a shear-lag unit [34], as illustrated in Fig. 6.

Liu et al. [34] fitted E_c to experimental results in a rearranged Equation (7), varying s, which they called effective aspect ratio (s_{eff}). The s_{eff} concept was useful for determining the mechanical percolation threshold (MPT) of GNP in the polymer. Besides, they showed that the thickness T of the composite interphase varies with the filler content in the composite. When the particles are far enough from each other, in low φ_f, the interphase thickness is as high as possible, according to the matrix shear modulus. But with the increase of φ_f, interphase regions of different particles start superposing, promoting a decrease in T.

From all the stated, we saw a different approach for Equation (7), which revealed itself particularly useful. Instead of substituting t/T by φ_f, we herein substituted φ_f by t/T in the equation to assess the thickness of interphase region. With that, the model, rearranged and considering the η_a coefficient, became Equation (8).

$$E_c \approx E_m\left[1-\frac{t}{T}+\frac{s^2}{12}\frac{\eta_o\eta_a}{(1+\nu)}\left(\frac{t}{T}\right)^2\right] \tag{8}$$

Thus, we calculated T for every sample, considering the same previously used parameters listed in Table S2, and the η_a coefficient of each composition. As shown in Fig. 7, the thickness of the interphase for both PVB/GO and PVB/MoS_2 nanocomposites decreased as a function of φ_f. Such behavior is akin to the observed by Liu et al. [34] for GNP in a thermoplastic elastomer through other approaches. Moreover, as the filler content decreases, better dispersion occurs, allowing the filler surface to be better covered by polymer chains that tend to align to said surface, which in turn leads to a thicker layer of highly "attached" molecules. On the other hand, the proximity of the filler neighboring particles and/or their agglomeration imply to the surface of the filler to be not that well covered and, consequently, a thinner layer of molecules to be affected by the filler. These correlations have been already demonstrated both theoretically [49] and experimentally [50].

4.3. Mechanical percolation threshold

Besides all the stated, it was possible to observe that the T decay with φ_f followed an exponential equation of the type $T = T_0 + Ae^{R_0\varphi_f}$. Consequently, an important implication is that, mathematically, the lowest possible thickness T of the interphase is T_0. Thus, in practice, T_0 is the theoretical thickness of the interphase at the mechanical percolation threshold. Therefore, it is possible to say that the filler volumetric fraction in which T tends to T_0 is the percolation threshold volume fraction of the filler (φ_p). Therefore, simplifying the math, φ_p can be easily calculated using Equation (9).

$$\varphi_p \approx \frac{\ln A}{-R_0} \tag{9}$$

By assessing PVB/GO percolation threshold volume fraction through Equation (9), a highly plausible φ_p of 0.93% or, by extent, a percolation threshold mass fraction of the filler (w_p) of 1.26%, was found. Such a value is right in between the 1.00 and 1.50 wt% range where a stagnation tendency of the nanocomposite Young's modulus was observed. Even more importantly for the plausibility of the found w_p, DMA showed that the area under the Cole-Cole curve increased with w_f up to 1.00% and decreased at higher loading, indicating the saturation of the reinforcement effect exactly as found through the MPT calculation. Lastly, the nanocomposite with 1.50 wt% was already too brittle to be easily handled, suggesting that PVB/GO nanocomposites with w_f higher than w_p would start losing mechanical properties. In turn, PVB/MoS_2 interphase T presented the same exponential decay behavior of PVB/GO with φ_f. Nevertheless, the notable agglomeration of the filler from a w_f as low

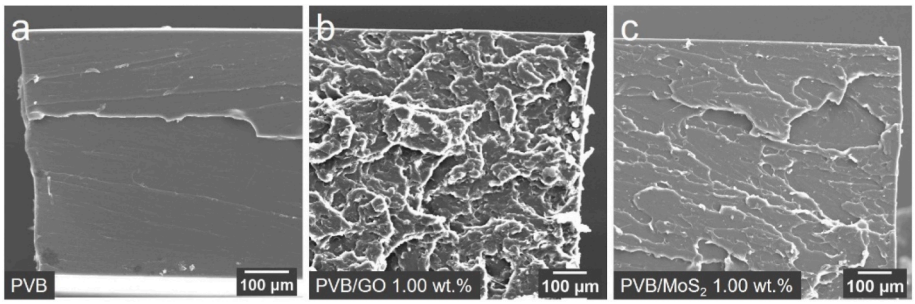

Fig. 4. SEM images of the fracture surface of a) PVB, b) PVB/GO 1.00 wt%, and c) PVB/MoS_2 1.00 wt%.

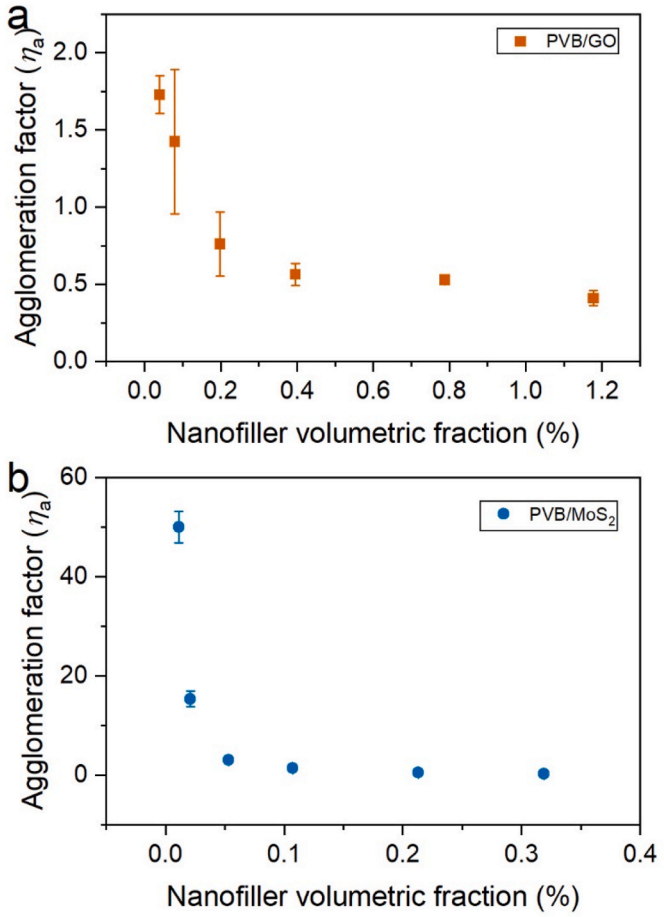

Fig. 5. Agglomeration coefficients (η_a) for the a) PVB/GO and b) PVB/MoS_2 nanocomposites.

Fig. 6. Scheme of (left) a shear-lag stress transfer unit for an individual flake within the polymeric matrix where t is the thickness of the flake and the T is the thickness of the portion of the matrix surrounding the flake, which the flake can affect when external stress is applied; and (right) the deformation of the flake and the matrix polymer after application of strain. Reproduced from Liu et al. [34].

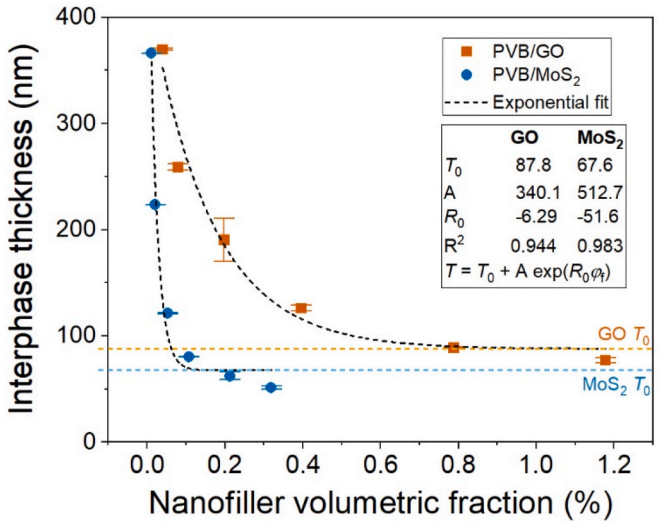

Fig. 7. Interface thickness (T) for the PVB/GO and PVB/MoS_2 nanocomposites.

as 0.10% made the interphase thickness drop considerably faster than that of PVB/GO with the φ_f increase as a clear consequence of the poor interaction MoS_2 with the polymer evidenced by FTIR and TGA. However, it is known that agglomerates of nanoparticles act as microparticles within polymeric matrices [48]. Hence, the φ_p of 0.12% (w_p of 0.61%) found through Equation (9) can be understood as the percolation threshold of the agglomerates, or the resulting "microparticles". In other words, for the determination of the actual φ_p of MoS_2, nanocomposites containing ultralow proportions of the filler, in the order of the employed by Rodriguez et al. [51], would have to be analyzed. In this case, MoS_2 flakes probably would remain isolated, acting as a reinforcement in the nanoscale. Even though, the found w_p of 0.61% also agreed with the DMA observation. It was shown that PVB/MoS_2 nanocomposite with w_f of 0.50%, was the one with the biggest E' in the glassy state and the largest area under the Cole-Cole plot. Thus, once again, the calculated w_p was close to the w_f in which DMA indicated the saturation of the reinforcement effect.

5. Conclusions

The mechanical reinforcement of PVB by GO and MoS_2 was analyzed. It was shown that GO physically interacted with the matrix through H-bonding, leading to a high degree of reinforcement. On the other hand, the poor interaction of MoS_2 with the matrix led to the agglomeration of the filler. Then, it was shown that the level of interaction between the polymer and the fillers was decisive in the mechanical behavior of the nanocomposites.

Moreover, the reinforcement mechanics of GO and MoS_2 in PVB were analyzed following a micromechanical analysis model from the

literature. An innovative look on the model allowed the thickness of the shear-lag units interphase to be mathematically assessed by the first time. It was also shown that T exponentially decreases with the volumetric fraction of the filler. This approach also allowed the assessment of the mechanical percolation threshold of GO and MoS_2 in PVB in a manner that could be closely related to DMA observations.

CRediT authorship contribution statement

Josué Marciano de Oliveira Cremonezzi: Conceptualization, Methodology, Validation, Formal analysis, Investigation, Data Curation, Discussion, Writing - Original Draft, Visualization.

Gabriel Matheus Pinto: Investigation, Discussion, Writing - Original Draft, Visualization.

Rosica Mincheva: Discussion.

Ricardo Jorge Espanhol Andrade: Discussion. Writing - Review & Editing.

Jean-Marie Raquez: Conceptualization, Validation, Resources, Discussion, Writing - Review & Editing.

Guilhermino José Macedo Fechine: Conceptualization, Validation, Resources, Writing - Review & Editing, Supervision, Project administration, Funding acquisition.

Declaration of competing interest

The authors declare that they have no known competing financial interests or personal relationships that could have appeared to influence the work reported in this paper.

Data availability

Data will be made available on request.

Acknowledgments

Funding: This work was supported by the Brazilian National Council for Scientific and Technological Development (CNPq) (processes 140241/2019-1, 307665/2018-6, and 305109/2022-7), Coordination of Superior Level Staff Improvement (CAPES), Brazil - Finance Code 001 [PrInt grant numbers 88887.583658/2020-00, and 88887.310339/2018–00], and The São Paulo Research Foundation (FAPESP) (processes 2020/11496-0 and 2021/07858-7). The study was also supported by the National Institute of Science and Technology of Carbon Nanomaterials of CNPq (INCT-Nanocarbono).

Appendix A. Supplementary data

Supplementary data to this article can be found online at https://doi.org/10.1016/j.compscitech.2023.110236.

References

[1] T.S. Valera, N.R. Demarquette, Polymer toughening using residue of recycled windshields: PVB film as impact modifier, Eur. Polym. J. 44 (2008) 755–768, https://doi.org/10.1016/j.eurpolymj.2007.12.012.

[2] Y. Bai, Y. Chen, Q. Wang, T. Wang, Poly(vinyl butyral) based polymer networks with dual-responsive shape memory and self-healing properties, J. Mater. Chem. A Mater. 2 (2014) 9169, https://doi.org/10.1039/c4ta00856a.

[3] A.M. Pandele, M. Ionita, L. Crica, S. Dinescu, M. Costache, H. Iovu, Synthesis, characterization, and in vitro studies of graphene oxide/chitosan–polyvinyl alcohol films, Carbohydr. Polym. 102 (2014) 813–820, https://doi.org/10.1016/j.carbpol.2013.10.085.

[4] E. Cascone, D.J. David, M.L. Di Lorenzo, F.E. Karasz, W.J. Macknight, E. Martuscelli, M. Raimo, Blends of polypropylene with poly(vinyl butyral), J. Appl. Polym. Sci. 82 (2001) 2934–2946, https://doi.org/10.1002/app.2149.

[5] M.D. Fernández, M.J. Fernández, P. Hoces, Synthesis of poly(vinyl butyral)s in homogeneous phase and their thermal properties, J. Appl. Polym. Sci. 102 (2006) 5007–5017, https://doi.org/10.1002/app.25004.

[6] Z.M. Zhou, D.J. David, W.J. Macknight, F.E. Karasz, Synthesis characterization and miscibility of polyvinyl butyrals of varying vinyl alcohol contents, Turk. J. Chem. 21 (1997) 229–238.

[7] A.K. Dhaliwal, J.N. Hay, The characterization of polyvinyl butyral by thermal analysis, Thermochim. Acta 391 (2002) 245–255, https://doi.org/10.1016/S0040-6031(02)00187-9.

[8] R.E. Mistler, E. Bianchi, B. Wade, J. Hurlbut, Evaluation of an environmentally friendly plasticizer for polyvinyl butyral for use in tape casting, in: Advanced Processing and Manufacturing Technologies for Structural and Multifunctional Materials: Ceramic Engineering and Science Proceedings, American Ceramic Society, Cocoa Beach, 2007, pp. 27–34.

[9] J. Xu, Y. Li, D. Ge, B. Liu, M. Zhu, Experimental investigation on constitutive behavior of PVB under impact loading, Int. J. Impact Eng. 38 (2011) 106–114, https://doi.org/10.1016/j.ijimpeng.2010.10.001.

[10] B. Liu, Y. Sun, Y. Li, Y. Wang, D. Ge, J. Xu, Systematic experimental study on mechanical behavior of PVB (polyvinyl butyral) material under various loading conditions, Polym. Eng. Sci. 52 (2012) 1137–1147, https://doi.org/10.1002/pen.22175.

[11] 360 Research Reports, Global PVB Film Sales Market Report 2020, 2020, pp. 1–143.

[12] G. Alva, Y. Lin, G. Fang, Thermal and electrical characterization of polymer/ceramic composites with polyvinyl butyral matrix, Mater. Chem. Phys. 205 (2018) 401–415, https://doi.org/10.1016/j.matchemphys.2017.11.046.

[13] K. Nakane, T. Kurita, T. Ogihara, N. Ogata, Properties of poly(vinyl butyral)/TiO2 nanocomposites formed by sol–gel process, Composites, Part B 35 (2002) 219–222, https://doi.org/10.1016/S1359-8368(03)00066-0.

[14] A.R. Zanjanijam, M. Hajian, G.A. Koohmareh, Fabrication of single wall carbon nanotubes-based poly(vinyl butyral) nanocomposites with enhanced mechanical and thermal properties, J. Macromol. Sci., Pure Appl. Chem. 51 (2014) 369–377, https://doi.org/10.1080/10601325.2014.882703.

[15] N. Stern, I. Dyamant, E. Shemer, X. Hu, G. Marom, Hybrid effects in the fracture toughness of polyvinyl butyral-based nanocomposites, Nanocompos. 4 (2018) 1–9, https://doi.org/10.1080/20550324.2018.1447827.

[16] X. Huang, Y. Lin, G. Fang, Thermal properties of polyvinyl butyral/graphene composites as encapsulation materials for solar cells, Sol. Energy 161 (2018) 187–193, https://doi.org/10.1016/j.solener.2017.12.051.

[17] J.C. Hoepfner, M.R. Loos, S.H. Pezzin, Evaluation of thermomechanical properties of polyvinyl butyral nanocomposites reinforced with graphene nanoplatelets synthesized by *in situ* polymerization, J. Appl. Polym. Sci. 135 (2018), 46157, https://doi.org/10.1002/app.46157.

[18] M. Hajian, M.R. Reisi, G.A. Koohmareh, A.R.Z. Jam, Preparation and characterization of polyvinylbutyral/Graphene nanocomposite, J. Polym. Res. 19 (2012), https://doi.org/10.1007/s10965-012-9966-6.

[19] K.S. Novoselov, V.I. Fal'ko, L. Colombo, P.R. Gellert, M.G. Schwab, K. Kim, A roadmap for graphene, Nature 490 (2012) 192–200, https://doi.org/10.1038/nature11458.

[20] A. Eftekhari, H. Garcia, The necessity of structural irregularities for the chemical applications of graphene, Mater. Today Chem. 4 (2017) 1–16, https://doi.org/10.1016/j.mtchem.2017.02.003.

[21] Z. Li, I.A. Kinloch, R.J. Young, The role of interlayer adhesion in graphene oxide upon its reinforcement of nanocomposites, Phil. Trans. Math. Phys. Eng. Sci. 374 (2016), 20150283, https://doi.org/10.1098/rsta.2015.0283.

[22] A.K. Singh, P. Kumar, D.J. Late, A. Kumar, S. Patel, J. Singh, 2D layered transition metal dichalcogenides (MoS_2): synthesis, applications and theoretical aspects, Appl. Mater. Today 13 (2018) 242–270, https://doi.org/10.1016/j.apmt.2018.09.003.

[23] X. Wang, W. Xing, X. Feng, B. Yu, L. Song, G.H. Yeoh, Y. Hu, Enhanced mechanical and barrier properties of polyurethane nanocomposite films with randomly distributed molybdenum disulfide nanosheets, Compos. Sci. Technol. 127 (2016) 142–148, https://doi.org/10.1016/j.compscitech.2016.02.029.

[24] J. Zhang, W. Lei, J. Schutz, D. Liu, B. Tang, C.H. Wang, X. Wang, Improving the gas barrier, mechanical and thermal properties of poly(vinyl alcohol) with molybdenum disulfide nanosheets, J. Polym. Sci. B Polym. Phys. 57 (2019) 406–414, https://doi.org/10.1002/polb.24799.

[25] K. Divya, M.S. Sri Abirami Saraswathi, D. Rana, S. Alwarappan, A. Nagendran, Custom-made sulfonated poly (ether sulfone) nanocomposite proton exchange membranes using exfoliated molybdenum disulfide nanosheets for DMFC applications, Polymer (Guildf.) 147 (2018) 48–55, https://doi.org/10.1016/j.polymer.2018.05.054.

[26] S. Stankovich, D.A. Dikin, G.H.B. Dommett, K.M. Kohlhaas, E.J. Zimney, E. A. Stach, R.D. Piner, S.T. Nguyen, R.S. Ruoff, Graphene-based composite materials, Nature 442 (2006) 282–286, https://doi.org/10.1038/nature04969.

[27] J.R. Potts, D.R. Dreyer, C.W. Bielawski, R.S. Ruoff, Graphene-based polymer nanocomposites, Polymer (Guildf.) 52 (2016) 145–160, https://doi.org/10.1016/j.polymer.2010.11.042.

[28] X. Sun, C. Huang, L. Wang, L. Liang, Y. Cheng, W. Fei, Y. Li, Recent progress in graphene/polymer nanocomposites, Adv. Mater. 33 (2021), 2001105, https://doi.org/10.1002/adma.202001105.

[29] T. Barkan, Graphene: the hype versus commercial reality, Nat. Nanotechnol. 14 (2019) 904–906, https://doi.org/10.1038/s41565-019-0556-1.

[30] T. Reiss, K. Hjelt, A.C. Ferrari, Graphene is on track to deliver on its promises, Nat. Nanotechnol. 14 (2019) 907–910, https://doi.org/10.1038/s41565-019-0557-0.

[31] D.G. Papageorgiou, I.A. Kinloch, R.J. Young, Mechanical properties of graphene and graphene-based nanocomposites, Prog. Mater. Sci. 90 (2017) 75–127, https://doi.org/10.1016/j.pmatsci.2017.07.004.

[32] R.J. Young, M. Liu, I.A. Kinloch, S. Li, X. Zhao, C. Vallés, D.G. Papageorgiou, The mechanics of reinforcement of polymers by graphene nanoplatelets, Compos. Sci. Technol. 154 (2018) 110–116, https://doi.org/10.1016/j.compscitech.2017.11.007.

[33] M. Liu, D.G. Papageorgiou, S. Li, K. Lin, I.A. Kinloch, R.J. Young, Micromechanics of reinforcement of a graphene-based thermoplastic elastomer nanocomposite, Composites Part A 110 (2018) 84–92, https://doi.org/10.1016/j.compositesa.2018.04.014.

[34] M. Liu, I.A. Kinloch, R.J. Young, D.G. Papageorgiou, Modelling mechanical percolation in graphene-reinforced elastomer nanocomposites, Compos. B Eng. 178 (2019), 107506, https://doi.org/10.1016/j.compositesb.2019.107506.

[35] J. Chu, R.J. Young, T.J.A. Slater, T.L. Burnett, B. Coburn, L. Chichignoud, A. Vuilleumier, Z. Li, Realizing the theoretical stiffness of graphene in composites through confinement between carbon fibers, Compos. Part A Appl Sci Manuf 113 (2018) 311–317, https://doi.org/10.1016/j.compositesa.2018.07.032.

[36] Z. Li, J. Chu, C. Yang, S. Hao, M.A. Bissett, I.A. Kinloch, R.J. Young, Effect of functional groups on the agglomeration of graphene in nanocomposites, Compos. Sci. Technol. 163 (2018) 116–122, https://doi.org/10.1016/j.compscitech.2018.05.016.

[37] C.S. Andrade, A.P.S. Godoy, M.A.G. Benega, R.J.E. Andrade, R.C. Andrade, W. M. Silva, J.M. de O. Cremonezzi, W.A. de A. Macedo, P.L. Gastelois, H. Ribeiro, J. Taha-Tijerina, Micro scalable graphene oxide productions using controlled parameters in bench reactor, Nanomaterials (2021), https://doi.org/10.3390/nano11081975, 1975.

[38] J.M. de O. Cremonezzi, H. Ribeiro, R.J.E. Andrade, G.J.M. Fechine, Characterization strategy for graphene oxide and molybdenum disulfide: proceedings based on the ISO/TS 21356-1:2021 standard, FlatChem 36 (2022), 100448, https://doi.org/10.1016/j.flatc.2022.100448.

[39] H. Liu, Y. Li, K. Dai, G. Zheng, C. Liu, C. Shen, X. Yan, J. Guo, Z. Guo, Electrically conductive thermoplastic elastomer nanocomposites at ultralow graphene loading levels for strain sensor applications, J. Mater. Chem. C Mater. 4 (2015) 157–166, https://doi.org/10.1039/c5tc02751a.

[40] K. Krishnamoorthy, M. Veerapandian, K. Yun, S.-J. Kim, The chemical and structural analysis of graphene oxide with different degrees of oxidation, Carbon N. Y. 53 (2013) 38–49, https://doi.org/10.1016/j.carbon.2012.10.013.

[41] K.-H. Liao, S. Aoyama, A.A. Abdala, C. Macosko, Does graphene change T_g of nanocomposites? Macromolecules 47 (2014) 8311–8319, https://doi.org/10.1021/ma501799z.

[42] A.K. Barick, D.K. Tripathy, Thermal and dynamic mechanical characterization of thermoplastic polyurethane/organoclay nanocomposites prepared by melt compounding, Mater. Sci. Eng. 527 (2010) 812–823, https://doi.org/10.1016/j.msea.2009.10.063.

[43] K. Wakabayashi, C. Pierre, D.A. Diking, R.S. Ruoff, T. Ramanathan, L. Catherine Brinson, J.M. Torkelson, Polymer - graphite nanocomposites: effective dispersion and major property enhancement via solid-state shear pulverization, Macromolecules 41 (2008) 1905–1908, https://doi.org/10.1021/ma071687b.

[44] D.G. Papageorgiou, I.A. Kinloch, R.J. Young, Graphene/elastomer nanocomposites, Carbon N. Y. 95 (2015) 460–484, https://doi.org/10.1016/j.carbon.2015.08.055.

[45] E.H.C. Ferreira, L.P. de Lima, G.J.M. Fechine, The “superlubricity state” of carbonaceous fillers on polymer composites, Macromol. Chem. Phys. (2020), 2000192, https://doi.org/10.1002/macp.202000192, 1–7.

[46] E.H.C. Ferreira, R.J.E. Andrade, G.J.M. Fechine, The “superlubricity state” of carbonaceous fillers on polyethylene-based composites in a Molten state, Macromolecules 52 (2019) 9620–9631, https://doi.org/10.1021/acs.macromol.9b01746.

[47] C.H. Mefford, Y. Qiao, M. Salviato, Failure behavior and scaling of graphene nanocomposites, Compos. Struct. 176 (2017) 961–972, https://doi.org/10.1016/j.compstruct.2017.06.013.

[48] M. Quaresimin, K. Schulte, M. Zappalorto, S. Chandrasekaran, Toughening mechanisms in polymer nanocomposites: from experiments to modelling, Compos. Sci. Technol. 123 (2016) 187–204, https://doi.org/10.1016/j.compscitech.2015.11.027.

[49] M.R. Gharib-Zahedi, A. Koochaki, M. Alaghemandi, Significantly Enhanced Polymer Thermal Conductivity by Confining Effect through Bilayer MoS2 Surfaces, 2021, pp. 1–20. http://arxiv.org/abs/2108.03875.

[50] E. Helal, L.G. Amurin, D.J. Carastan, R.R. de Sousa, E. David, M. Fréchette, N. R. Demarquette, Interfacial molecular dynamics of styrenic block copolymer-based nanocomposites with controlled spatial distribution, Polymer (Guildf.) 113 (2017) 9–26, https://doi.org/10.1016/j.polymer.2017.02.025.

[51] C.L.C. Rodriguez, M.A.B.S. Nunes, P.S. Garcia, G.J.M. Fechine, Molybdenum disulfide as a filler for a polymeric matrix at an ultralow content: polystyrene case, Polym. Test. 93 (2021), https://doi.org/10.1016/j.polymertesting.2020.106882 undefined.